SEASONAL VARIABILITY OF AIR INFILTRATION RATES IN BUILDINGS WITH DIFFERING AIRTIGHTNESS

*Kovač B., **Vaupotič J., *Dovjak M.

*Faculty of Civil and Geodetic Engineering, University of Ljubljana, Ljubljana, Slovenia

**Jožef Stefan Institute, Ljubljana, Slovenia
bruno.kovac@fgg.uni-lj.si

Abstract. This study investigates the seasonal variability of air infiltration rates (N_{inf}) in two residential buildings with differing envelope airtightness (B1: older, lower; B2: newer, higher). N_{inf} were quantified using the CO₂ decay method in February and June 2025. N_{inf} were higher and more variable (B1: 0.14–0.27 h^{-1} , avg 0.19 h^{-1} ; B2: 0.04–0.21 h^{-1} , avg 0.10 h^{-1}) in winter and lower (B1: 0.06–0.25 h^{-1} , avg 0.13 h^{-1} ; B2: 0.00–0.22 h^{-1} , avg 0.06 h^{-1}) in summer. N_{inf} decreased with increasing outdoor temperature, with meteorological influences more evident in the less airtight building.

Key Words: Air infiltration rate, CO_2 decay method, seasonal variability.

Introduction

The construction of energy-efficient buildings relies on achieving enhanced airtightness of the building envelope, which reduces uncontrolled heat losses and supports the optimal indoor air quality (IAQ) through the integration of an efficient ventilation system. However, approximately 75% of the existing building stock comprises older buildings with lower envelope airtightness, creating ongoing challenges for improving energy performance and maintaining adequate IAQ [1].

A key indicator of building envelope airtightness is the air infiltration rate ($N_{\rm inf}$), which quantifies the uncontrolled inward leakage of air into spaces through unintended openings in ceilings, floors, and walls. Driven by pressure, resulting from wind, temperature gradients (stack effect), and mechanical imbalances, air infiltration increases heating and cooling demand, leading to higher energy use, introduces outdoor pollutants, and causes drafts that reduce thermal comfort [2,3]. Its magnitude depends on the building age, materials and construction quality, with older buildings typically exhibiting 0.25–0.60 air changes per hour (ACH) under normal conditions, compared to 0.10–0.23 ACH in newly constructed buildings [4,5].

In newly constructed buildings, airtightness is typically assessed using the standardised blower door test, a static method defined by EN ISO 9972:2015 [6], which measures leakage under a pressure differential of 50 pascals between the interior and exterior of the building envelope. While helpful in benchmarking, this static test does not reflect the dynamic effects of wind, temperature fluctuations, or material ageing, all of which alter leakage pathways over time [7,8]. In contrast, the tracer gas method (i.e., CO₂, SF₆) enables long-term, non-intrusive monitoring under natural conditions, capturing seasonal variability. Comparative studies have shown that tracer gas approaches yield up to 38% greater accuracy and lower uncertainty than blower door measurements [7,8].

Given these considerations, the present study investigates seasonal variations in air infiltration rates in two residential buildings with differing levels of airtightness. The objectives are: (1) to quantify air infiltration rates in winter and summer; (2) to monitor meteorological parameters simultaneously; (3) to evaluate the influence of weather conditions on infiltration dynamics; and (4) to compare seasonal differences between buildings.

Study area, material and methods

The study was conducted in two residential buildings with differing airtightness: B1, a multi-apartment building constructed in 2000 with lower airtightness, and B2, a single-family house built in 2014 with higher airtightness. Measurements were performed in one room per building, with net volumes 64 m³ (B1) and 33 m³ (B2).

Air infiltration rates ($N_{\rm inf}$, expressed as air changes per hour, h⁻¹) were determined using the tracer gas method, specifically the CO₂ decay technique [9]. Measurements were conducted in closed and unoccupied spaces on working days between 8:00 and 16:00 in February (winter) and June 2025 (summer), producing four datasets (B1 and B2 in winter and summer). Indoor CO₂ concentrations were monitored using a HOBO® MX Logger, while indoor air temperature and relative air humidity were recorded with an AirLink 7212 sensor. Outdoor meteorological data (air temperature, wind speed, relative air humidity, and precipitation) were obtained from the Slovenian Environment Agency (ARSO).

Data processing and statistical analysis were performed using RStudio. For each dataset, avg $N_{\rm inf}$ values were calculated within the measurement window. Ventilation heat losses for heating and non-heating seasons were calculated using KI Energija software. Descriptive statistics, Pearson correlation coefficients with significance levels (p-values) for $N_{\rm inf}$ versus monitored parameters, and ratios of seasonal and inter-buildings differences were computed. Results were visualized as (1) seasonal average hourly values to compare daily patterns across buildings and seasons, and (2) diurnal variations on selected days to illustrate short-term fluctuations.

Results

Fig. 1a shows the winter and summer variability of average hourly air infiltration rates ($N_{\rm inf}$), while Fig. 1b presents outdoor air temperature ($T_{\rm outdoor}$) for B1 (low-airtight envelope) and B2 (high-airtight envelope) during February and June 2025 (B1_Feb, B1_Jun, B2_Feb, B2_Jun). $N_{\rm inf}$ were consistently higher in February than in June across B1 and B2, confirming the seasonal effect. A decreasing diurnal trend was observed across all datasets, indicating reduced air infiltration during warmer afternoon hours. The distribution of $N_{\rm inf}$ values also varied by building and season. In B1, the range was wider in June (0.10–0.19 h⁻¹) than in February (0.16–0.22 h⁻¹), reflecting greater within-day variability during summer. This pattern aligned with the broader temperature span in June compared with February. In B2, the $N_{\rm inf}$ values showed a narrower distribution and weaker seasonally contrasts, with ranges of 0.09–0.11 h⁻¹ in February and 0.05–0.08 h⁻¹ in June. $T_{\rm outdoor}$ showed a steady daytime increase, with June averages (24.0 °C in B1, 23.0 °C in B2) approximately 15–20 °C higher than those in February (4.0 °C in B1, 5.7 °C in B2).

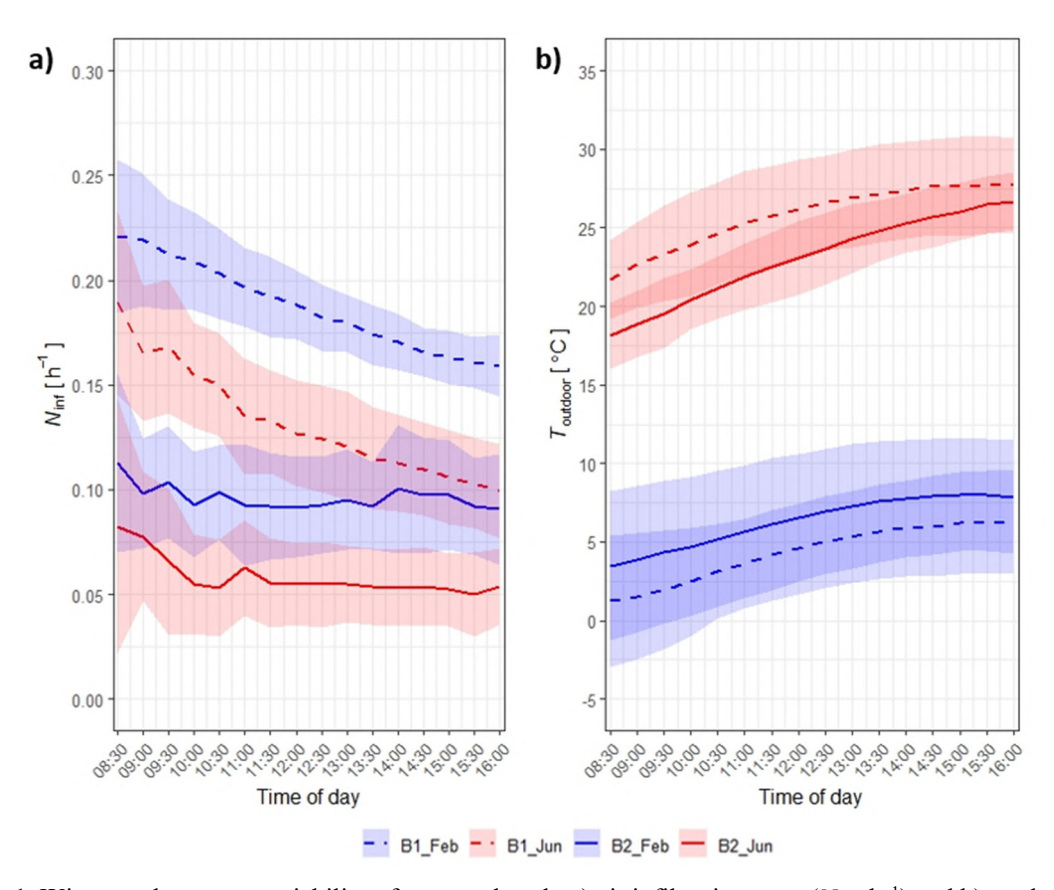


Fig. 1. Winter and summer variability of average hourly a) air infiltration rates (N_{inf}, h^{-1}) and b) outdor air temperature $(T_{outdoor}, {}^{\circ}C)$ for two buildings with differing airtightness (B1_Feb, B1_Jun, B2_Feb, B2_Jun).

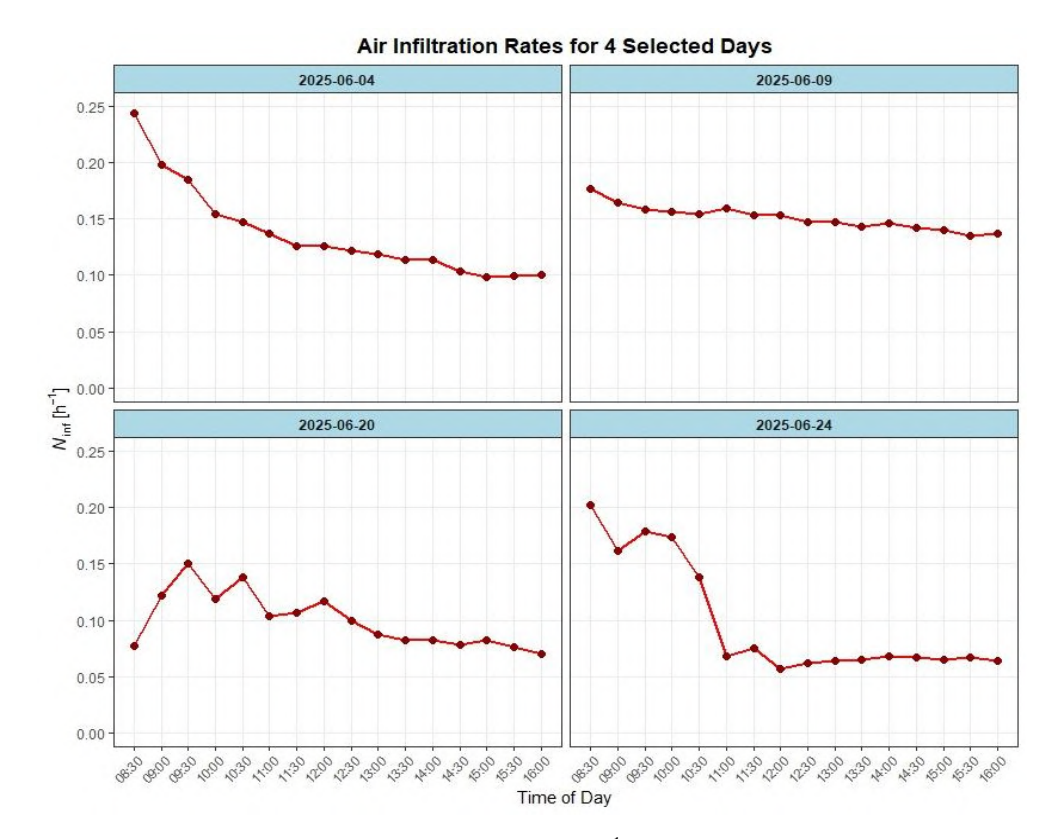


Fig. 2. Diurnal variations of air infiltration rates (N_{inf}, h^{-1}) in four selected days in B1, June 2025.

Fig. 2 illustrates the diurnal variation of N_{inf} in B1 across four representative days in June 2025 (4th, 9th, 20th, and 24th), highlighting differences in short-term fluctuations driven by meteorological conditions. On June 4th, a pronounced decrease in N_{inf} , (from 0.25 to 0.10 h⁻¹) was observed, associated with higher wind speed ($> 3.0 \text{ m s}^{-1}$), which suppressed N_{inf} . On June 9th, N_{inf} remained relatively high and stable (0.17–0.14 h^{-1}), likely due to lower T_{outdoor} . June 20th exhibited moderate variability, with peak values reaching 0.15 h^{-1} and a subsequent decline to 0.07 h^{-1} . In contrast, June 24^{th} showed the sharpest drop in N_{inf} , decreasing from 0.20 h^{-1} in the morning to 0.06 h^{-1} by noon, after which the values remained low. On both days, N_{inf} reflected the combined influence of Toutdoor and wind speed.

Across buildings, the variability of $N_{\rm inf}$ was driven by different meteorological parameters. In B1, $N_{\rm inf}$ was primarily influenced by T_{outdoor} (p=-0.69), followed by the outdoor/indoor temperature difference (T_{diff}) and air pressure in February, and by T_{diff} and relative humidity (RH) in June. In B2, T_{outdoor} had a weaker effect on $N_{\rm inf}$ (p=-0.16 in February; -0.33 in June), while stronger drivers included RH and $T_{\rm diff}$ in February, and air pressure and wind speed in June. These building-specific drivers may explain the observed diurnal fluctuations.

Table 1 summarises statistics on calculated $N_{\rm inf}$ and measured $T_{\rm outdoor}$ in B1 and B2 during February and June 2025, along with winter-to-summer ratio analysis.

			1	Contacol	,			8		
	Basic statistics of calculated and measured data								Seasonal N _{inf} ratio	
	B1_Feb		B2_Feb		B1_Jun		B2_Jun		winter / summer	
	$N_{\rm inf}$	$T_{ m outdoor}$	N_{inf}	$T_{ m outdoor}$	$N_{ m inf}$	$T_{ m outdoor}$	N_{inf}	$T_{ m outdoor}$	B1_Feb/	B2_Feb /
									B1_Jun	B2_Jun
MIN	0.14	-5.4	0.04	-3.7	0.06	14.3	0.00	12.4	2.33	*
MAX	0.27	12.2	0.21	15.1	0.25	33.0	0.22	29.8	1.08	0.95

6.3

4.3

-0.16

AVG

STDEV

 $p\ (N_{
m inf},\, T_{
m outdoor})$

0.19

0.03

4.3

3.6

-0.69

0.10

0.03

Table 1. Statistical analysis and ratios of air infiltration rates (N_{inf}) and outdoor temperatures (T_{outdoor}) for different seasons and buildings.

0.13

0.04

25.8

-0.61

3.5

0.06

0.03

23.0

3.4

-0.33

1.46

0.75

1.67

1.00

 N_{inf} values exhibited considerable variability across seasons and buildings, ranging from 0.00 h⁻¹ (B2_Jun minimum) to 0.27 h⁻¹ (B1_Feb maximum). In B1, February values ranged from 0.14 to 0.27 h⁻¹ (avg 0.19 h⁻¹), while June values ranged from 0.06 to 0.25 h⁻¹ (avg 0.13 h⁻¹). Similarly, B2 showed a February range of 0.04 to 0.21 h⁻¹ (avg 0.10 h⁻¹), and a June range of 0.00 to 0.22 h⁻¹ (avg 0.06 h⁻¹). The winter-to-summer ratios further highlight this pattern: in B1 it was 1.46, and in B2 1.67, indicating that winter air infiltration was approximately 1.5 to 1.7 times higher than in summer. When comparing the two buildings, B1 consistently exhibited higher infiltration rates than B2, with values being 1.9 times higher in February and 2.2 times higher in June. Correlation coefficients between N_{inf} and T_{outdoor} ranged from -0.16 (B2_Feb) to -0.69 (B1_Feb), confirming a moderate to strong inverse relationships. Higher air infiltration rates in B1 during winter (avg 0.19 h⁻¹) compared to B2 (avg 0.10 h⁻¹), combined with its larger room volume of B1, resulted in significantly greater ventilation heat losses: 57 kWh in B1 versus 15 kWh in B2 during February.

Conclusion

Air infiltration rates, determined using the CO₂ decay method, exhibited seasonal and inter-building differences in two residential buildings (B1, B2) with contrasting airtightness. Winter air infiltration rates consistently exceeded summer values, with winter-to-summer ratios ranging from 1.46 (B1) to 1.67 (B2). Airtightness governed the overall magnitude of air infiltration, while outdoor air temperature emerged as the primary dynamic driver, particularly in B1 with its less airtight envelope, where the correlation coefficient reached –0.69. These findings are consistent with previous studies [4,5,10].

Tracer gas (CO₂) monitoring under natural operating conditions effectively captured temporal variations in air infiltration, thereby complementing standardised tests by reflecting real building performance. The results highlight that an airtight envelope can reduce uncontrolled air infiltration and ventilation heat losses, supporting more stable indoor environments across seasons.

References

- 1. European Commission. Energy Performance of Buildings Directive. // European Commission, 2024. Available at: https://energy.ec.europa.eu/topics/energy-efficiency/energy-efficient-buildings/energy-performance-buildings-directive en [Accessed 25 September 2025].
- 2. ASHRAE. ANSI/ASHRAE Standard 62.1 2022. Ventilation and Acceptable Indoor Air Quality. // American Society of Heating, Refrigerating and Air-Conditioning Engineers, Atlanta, GA, 2022.
- 3. Lu, Y., Xiang, Y., Chen, G., Liu, J., & Wang, Y., On-site measurement and zonal simulation on winter indoor environment and air infiltration in an atrium in a severe cold region. // Energy and Buildings, v. 223, 2020, 110160. https://doi.org/10.1016/j.enbuild.2020.110160.
- 4. Ji, Y., Duanmu, L., Liu, Y., & Dong, H., Air infiltration rate of typical zones of public buildings under natural conditions. // Sustainable Cities and Society, v. 61, 2020, 102290. https://doi.org/10.1016/j.scs.2020.102290.
- 5. Du, Y., Ji, Y., Lin, D., & Hu, S., A case study of air infiltration for highly airtight buildings under the typical meteorological conditions of China. // Buildings, v. 14, 2024, 1585. https://doi.org/10.3390/buildings14061585.
- 6. EN ISO 9972:2015. Thermal performance of buildings Determination of air permeability of buildings Fan pressurization method. // European Committee for Standardization, Brussels, 2015.
- Patel, T., Mitsingas, C., Miller, J., & Newell, T., Comparison of blower door and tracer gas testing methods for determination of air infiltration rates through building envelopes at normal operating conditions. // ASME Energy Sustainability Conference, 2011, pp. 1013–1019. https://doi.org/10.1115/ES2011-54373.
- 8. Undram, M., Song, D., & Kim, J., A review of the test methods for airtightness performance of building components using the blower door system. // Korean Journal of Air-Conditioning and Refrigeration Engineering, v. 31, 2019, p. 216. https://doi.org/10.6110/KJACR.2019.31.5.216.
- 9. Shi Y., Li X., A convenient method to assess air infiltration rate using particle mass balance principle. // E3S Web of Conferences, v. 111, 2019, 06039. https://doi.org/10.1051/e3sconf/201911106039.
- 10. Younes, C. Air infiltration through building envelopes: A review. Indoor and Built Environment, v. 21, 2012, pp. 142–157. https://doi.org/10.1177/1744259111423085.